

Method of directional spectrum estimation accounting for the ambient shearing currents

Rotem Soffer¹,* Eliezer Kit¹,† and Yaron Toledo¹,‡

Tel-Aviv University, School of Mechanical Engineering, Haim Levanon 55, Tel Aviv, Israel



(Received 19 November 2022; accepted 12 May 2023; published 30 June 2023)

Realistic currents in seas and oceans are almost always changing in depth thus indicative on the presence of shear in the profile of the mean ambient flow. However, analysis methodologies interpreting directional wave data gathered by *in situ* measurement instruments such as buoys, pressure gauges, and acoustic Doppler current profilers (ADCPs) utilize potential irrotational flow theory which cannot account for the rotational shearing currents. The effects of shearing currents on the wave direction estimations were studied on numerically simulated ADCP data of waves propagating in a predetermined spread. The numerical data was generated employing the Rayleigh boundary-value problem (BVP) and a selected ambient current profile. The potential data processing led to significant errors in wave directional spread estimation for common shearing currents (up to $\approx 10^\circ$ in mean wave direction for the presented example). This finding is of great importance because it addresses the influence of an ambient current profile on wave propagation direction. The obtained results suggest that there is an uncertainty with the confidence of any wave directional spread ever presented by *in situ* wave measurement devices. Here, we developed an approach for estimating directional wave spectra based on rotational flow physics by acquiring terms emanating from wave-shearing current interaction governing equations. This included a derivation of numerical transfer functions for the fluid's physical properties based on the Rayleigh BVP. Then, by applying classical cross- and auto-spectral analysis on time-series data sets, the directional spread function was numerically reconstructed. This derived data processing methodology was applied to the same numerically simulated ADCP data sets. It was found to be capable of reconstructing the spread with great accuracy (0.4° in mean wave direction for the presented example). This makes it a prominent methodology for estimating directional wave spectra in realistic oceanic conditions.

DOI: [10.1103/PhysRevFluids.8.L062801](https://doi.org/10.1103/PhysRevFluids.8.L062801)

The wind wave directional spread function is a key parameter in characterizing a wave field. It has many implications for oceanographic, environmental, and maritime engineering applications. Statistics of wave heights and periods can be directly reproduced just from a single analog record of the sea elevation. However, the estimation of the wave direction is more complex especially for *in situ* measurement sensors, such as directional wave buoys, current meters, or wave gauge arrays. There are several types of sea measurement instruments and sensors providing estimation for the wave directional spectrum. Their records are processed according to wave potential theory, where the random sea wave motion is described as weakly stationary, and ergodic random stochastic process.

*rotemsof@mail.tau.ac.il

†kit@tauex.tau.ac.il

‡toledo@tauex.tau.ac.il

Originally, wave directional spectrum estimations were carried out by deploying an array of bottom pressure gauges. Cross-spectra products were conducted between the gauges, and the known distances between them completed the required information. As the number of pressure gauges increased, the wave directional spectrum resolution improved. Optimal pressure sensor array shapes were suggested by Refs. [1,2]. Longuet-Higgins invented a pitch-roll buoy—the first *in situ* point sensor instrument supplying the directional wave spectrum. This buoy provided three datasets: sea elevation record obtained by an accelerometer mounted on a gimbal and pitch and roll records obtained by two gyroscopes [3]. Kuik developed a model-free parameters processing method for buoys [4], relying on the previous works of Refs. [5,6]. Nowadays, wave rider buoys equipped with vertical and horizontal accelerometers are common and their data processing is carried out in a similar manner [7–9].

Another technique to estimate the directional spreading function is to measure the pressure and two components of the wave oscillatory velocities (commonly referred to as PUV). It is suitable for measurement of wave directions in areas of finite water depth. The basic principle for estimating the directional wave spectra by PUV is similar to that of the pitch-roll buoy. One of the frequently employed PUV-meter instruments is acoustic Doppler current profiler (ADCP). The horizontal oscillatory velocities are related to the sea elevation by applying transfer functions defined according to potential wave theory similarly to buoys:

$$K_p(\omega, z) = \rho g \frac{\cosh k(z+h)}{\cosh kh}, \quad (1)$$

$$K_c(\omega, z) = \omega \frac{\cosh k(z+h)}{\sinh kh}. \quad (2)$$

Here, $K_p(\omega)$ is the transfer function for the pressure, $K_c(\omega)$ is the transfer function for the oscillatory horizontal velocity measurements, ω is the wave radial frequency, z is the sensor level, and h is the bottom depth. The wave numbers k are calculated according to potential dispersion relation over a constant depth. In later generations of ADCPs, the sea elevation is measured directly by an acoustic surface tracking (AST) vertical beam not requiring (1) (commonly referred to as SUV). Statistical approaches have been studied to improve the directional spread function estimation (see Ref. [10]) including the popular maximum likelihood method (MLM) [11–15]. Wave directional spectra are widely employed in data assimilation in numerical meteorological forecast models. Statistical analysis of mean wave parameters clearly shows that the use of spectral information yields a better estimate of wave frequency, direction, and low-frequency wave height in comparison with the results based upon assimilation of wave heights only in WAM model [16]. Recently, the Sofar Spotter network, which is composed of over 600 globally distributed, free-drifting marine weather buoys [17–19], were employed the first operational spectral wave data assimilation, improving forecast accuracy of bulk parameters and spectral characteristics [20]. The conventional methods for estimating the directional spectrum from measurements conducted by wave gauge arrays, directional wave buoys, and ADCPs employ potential flow theory. This means that only zero or uniform ambient currents can be accounted for. Nevertheless, in common oceanic flows the ambient currents can change in depth (vertically shearing currents) significantly affecting the oscillatory wave properties including the dispersion relation (see, e.g., Ref. [21] for nonviscous flows and Ref. [22] for turbulent flows). Recent works employed rotational theory of second order and studied the probability of rogue waves obtained from measurements and found that waves are significantly reduced and enhanced during ebb and flood [23]. That research followed previous studies [24,25] and led the author to conclude that shearing currents need to be accounted for in wave modeling and prediction.

Although the theory relating the waves to shearing currents has existed for almost 50 years, this effect has not been accounted for in data processing of directional wave spectra obtained by wave buoys, pressure gauges, and ADCPs. The current study shows that the wave directional spectrum processed using potential theory has significant flaws for realistic oceanic flow conditions.

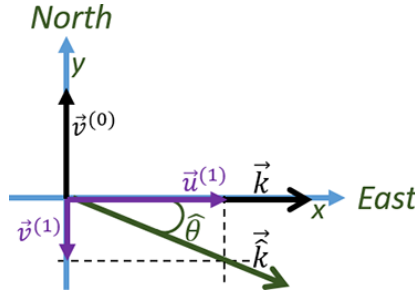


FIG. 1. Example of monochromatic wave \vec{k} propagating in x direction in the presence of perpendicular linear shearing current $v^{(0)}(z)$. The error of the estimated wave direction $\hat{\theta}$ according to potential theory is related to the simple projection caused by the actual first-order velocities $u^{(1)}(z)$, $v^{(1)}(z)$, forcing \vec{k} to be aligned with them.

In potential theory, shearing current effects cannot be accounted for due to the theory's inherent irrotationality. To demonstrate the limitation of the potential approach in wave directionality estimation, a simplified case of a monochromatic wave propagating in the x direction in the presence of a perpendicular linear current $v^{(0)}(z)$ applied in the y direction (see Fig. 1) is presented. The linear current is $v^{(0)}(z) = \alpha(h + z) + \beta$ with z varying in $[-h, 0]$, and α and β are constant coefficients. The wave physical oscillating parameters in the presence of shearing currents are related each to other due to interaction terms showing their mutual dependence [26] via Rayleigh boundary-value problem (BVP); see, e.g., Ref. [27], and also described in detail in the Supplemental Material [26]. The BVP's solution for the oscillating horizontal velocity vector $\vec{U}^{(1)}(z) = [u^{(1)}, v^{(1)}]^T$ is defined via the oscillating vertical velocity $w^{(1)}(z)$ and the mean horizontal velocity $\vec{U}^{(0)}(z) = [u^{(0)}, v^{(0)}]^T$ as

$$\vec{U}^{(1)} = \frac{i \vec{k} \omega_d}{k^2} \frac{\partial}{\partial z} \left(\frac{w^{(1)}}{\omega_d} \right) - \frac{i w^{(1)}}{\omega_d} \frac{\partial \vec{U}^{(0)}}{\partial z}, \quad (3)$$

where ω_d is the intrinsic frequency. At first glance one may think that as the wave is perpendicular to the ambient flow, it should not be affected, and indeed the Rayleigh equation for linear shearing current is degenerated to the homogeneous Laplace's equation (as in the potential case). Since the chosen shearing flow is orthogonal to the wave propagation direction, the dispersion relation also remains as in the potential case, and $\omega_d(z) = \omega$. Nevertheless, in further inspection, the oscillatory flow has a horizontal component in the perpendicular direction $v^{(1)}$ which does not appear under irrotational assumptions (3), since $\partial \vec{U}^{(0)}/\partial z$ is zero in potential case. This means that potential flow data analysis neglecting the wave-current interaction has an inherent problem of accurately predicting wave directionality. According to the potential approach the estimated wave propagation direction $\hat{\theta}$ will be aligned with $\vec{U}^{(1)}(z)$ and will differ from the actual predetermined direction $\theta = 0^\circ$. The error is dependent on the shear slope magnitude and the wave period and length as follows:

$$\hat{\theta} - \theta = \arctan \left(\frac{v^{(1)}|_{z=0}}{u^{(1)}|_{z=0}} \right) = \arctan \left(\frac{-\alpha \tanh kh}{\omega} \right). \quad (4)$$

For a wave of $T = 10$ s, $h = 10$ m, and a slope of $\alpha = 0.1 \text{ s}^{-1}$, the error in the estimation is -5.4° , so the potential interpretation is that the wave is approaching from a more northern direction. This simplified example demonstrates the necessity in accounting for the shearing current to avoid errors in directional analysis. In this Letter we present an interpretation methodology based on rotational flow theory instead of a potential one. It manages to more accurately estimate the directional wave spectra and specifically the mean wave direction, while accounting for the ambient shearing

current effects. We introduce a processing method for wave directional power density spectrum estimation based on the Rayleigh BVP. It also provides a more accurate dispersion relation. The linear description of the sea elevation $\eta(x, y, t)$ is

$$\eta(x, y, t) = \int_{\omega} \int_{\theta} \eta^{(1)}(\partial\omega, \partial\theta) P(x, y, t), \quad (5)$$

$$P(x, y, t) = \exp [i(k \cos \theta x + k \sin \theta y - \omega t + \phi)], \quad (6)$$

where $\eta^{(1)}(\partial\omega, \partial\theta)$ is the wave amplitude. As stated by Refs. [7,14], from the physical point of view, $\eta^{(1)}(\partial\omega, \partial\theta)$ means the amplitude which represents the energy within intervals $[\omega, \omega + \partial\omega]$ and $[\theta, \theta + \partial\theta]$. These wave amplitudes are proportional to $\sqrt{\partial\omega\partial\theta}$. Other physical properties are noted as $\xi(x, y, z, t)$,

$$\xi(x, y, z, t) = \int_{\omega} \int_k \xi^{(1)}(\partial\omega, \partial\theta, z) P(x, y, t), \quad (7)$$

$$\xi^{(1)}(\partial\omega, \partial\theta, z) = H_{\xi}(\omega, \theta, z) \eta^{(1)}(\partial\omega, \partial\theta). \quad (8)$$

Here, $H_{\xi}(\partial\omega, \partial\theta, z)$ is a transfer function establishing the relation between η and any physical property ξ , such as horizontal velocities, vertical velocity, accelerations, pressure, etc. It is computed using

$$H_{\xi_{\omega,\theta,z}}^s = \frac{\int_{\omega}^{\omega+\Delta\omega} \int_{\theta}^{\theta+\Delta\theta} \xi^{(1)}(\partial\omega, \partial\theta, z)}{\int_{\omega}^{\omega+\Delta\omega} \int_{\theta}^{\theta+\Delta\theta} \eta^{(1)}(\partial\omega, \partial\theta)} = \frac{\xi_{\omega,\theta,z}^{(1)}}{\eta_{\omega,\theta}^{(1)}}, \quad (9)$$

where $\xi_{\omega,\theta}^{(1)}$ is the oscillatory amplitude of any wave physical property, and $\eta_{\omega,\theta}^{(1)}$ is the surface elevation amplitude. We evaluated the transfer function $H_{\xi}(\partial\omega, \partial\theta, z)$ accounting for the shearing currents in accordance to numerical solutions of the BVP substituted in (9) to replace the potential transfer functions. The case of an ADCP employing of three data-sets of pressure and horizontal velocities PUV is reviewed. The transfer functions $H_{i_{\omega,\theta}}^s$ were derived using (9) together with the BVP solutions. After some mathematical simplifications, they take the form

$$H_{p_{\omega,\theta}}^s(z) = \alpha_{\omega,\theta}(z) r(\theta), \quad (10)$$

$$H_{u_{\omega,\theta,z}}^s + 2c_{\omega,\theta,z}^{(3)} = r(\theta) \cos \theta, \quad (11)$$

$$H_{v_{\omega,\theta,z}}^s + 2c_{\omega,\theta,z}^{(2)} = r(\theta) \sin \theta, \quad (12)$$

$$r(\theta) = \{c_{\omega,\theta,z}^{(1)} + 2[c_{\omega,\theta,z}^{(3)} \cos \theta + c_{\omega,\theta,z}^{(2)} \sin \theta]\}, \quad (13)$$

with the $c^{(i)}$ coefficients defined at the measurement depth $z = z_0$ as

$$c_{\omega,\theta}^{(1)}(z_0) = \frac{\frac{\partial w_{\omega,\theta}^{(1)}(z_0)}{\partial z} \omega_{d_{\omega,\theta}}(0)}{k_{\omega,\theta} w_{\omega,\theta}^{(1)}(0)}, \quad (14)$$

$$c_{\omega,\theta}^{(2)}(z_0) = \frac{\frac{\partial v_{\omega,\theta}^{(1)}(z_0)}{\partial z} w_{\omega,\theta}^{(1)}(z_0) \omega_{d_{\omega,\theta}}(0)}{2w_{\omega,\theta}^{(1)}(0) \omega_{d_{\omega,\theta}}(z_0)}, \quad (15)$$

$$c_{\omega,\theta}^{(3)}(z_0) = \frac{\frac{\partial u_{\omega,\theta}^{(1)}(z_0)}{\partial z} w_{\omega,\theta}^{(1)}(z_0) \omega_{d_{\omega,\theta}}(0)}{2w_{\omega,\theta}^{(1)}(0) \omega_{d_{\omega,\theta}}(z_0)}, \quad (16)$$

$$\alpha_{\omega,\theta}(z_0) = \frac{\rho \omega_{d_{\omega,\theta}}(z_0)}{k_{\omega,\theta}}. \quad (17)$$

$c_{\omega,\theta}^{(i)}(z_0)$ are discrete coefficients that are calculated numerically via the solution of the BVP for each wave radial frequency ω and direction θ .

For the simplified case without a current, $c_{\omega,\theta,z_0}^{(2)}, c_{\omega,\theta,z}^{(3)} \rightarrow 0$, the radius $r(\theta)$ does not depend on θ , and the transfer functions degenerate to the potential ones K_p, K_c defined in (1) and (2). In this case, the direction of $\vec{U}^{(1)}$ coincides with the one of the wave \vec{k} . This results in a simple polar projection of the velocity vector on the x and y directions, i.e., $\cos \theta$ and $\sin \theta$, respectively, as seen in equations (11) and (12). When waves propagate in the presence of a shearing current, $c_{\omega,\theta}^{(2)}$ and $c_{\omega,\theta}^{(3)}$ do not vanish and $r(\theta)$ depends on θ . The transfer functions depend on the ambient current $\vec{U}^{(0)}$ and its shear $\partial \vec{U}^{(0)}/\partial z$ as seen in (15) and (16). The pressure transfer function (10) depends now on θ preventing the simple use of K_p . For the horizontal velocity transfer functions (11) and (12), this results in a more complex projection that corrects the deviation caused by $\vec{U}^{(1)}$ assumed by the potential approach.

Cross-spectra of two time series $\xi_m(t), \xi_l(t)$ (7) can be described as a reconstruction of a Fourier series with unknown Fourier coefficients \hat{a}_n, \hat{b}_n . The cross-spectra products per frequency ω are summed over all directions for a predetermined directional discretization step $\Delta\theta$ in order to employ the rotational derived transfer functions (9)

$$[S_{ml}]_{\omega} = S_{\omega} \sum_{\theta} H_{m,\omega,\theta,z}^s H_{l,\omega,\theta,z}^{s*} \frac{1}{\pi} \left[\frac{1}{2} + \sum_n (\hat{a}_n \cos(n\theta) + \hat{b}_n \sin(n\theta)) \right] \Delta\theta. \quad (18)$$

A pair of m, l independent measurement records can yield two auto-spectra and one cross-spectrum equations. The number of Fourier coefficients that can be solved is dependent on the number of the independent records. The solution of the Fourier coefficients enables constructing the directional spread function for a selected frequency

$$S_{\omega}(\theta) = S_{\omega} \frac{1}{\pi} \left[\frac{1}{2} + \sum_n (\hat{a}_{n\omega} \cos(n\theta) + \hat{b}_{n\omega} \sin(n\theta)) \right]. \quad (19)$$

An example of an application of the developed methodology is shown by employing numerically simulated data. We generated three data-sets as ADCP records employing an AST beam providing time-series of the surface elevation η and east and north horizontal velocities u, v (SUV). The use of artificially simulated data for testing the methodology has a great advantage since it enables comparison between the predefined directional wave spectrum with the reconstructed one. A similar approach was successfully used in studies of turbulence [28,29]. The case of an ADCP was chosen since it is capable of providing the ambient current record $u^{(0)}, v^{(0)}$, the oscillatory records $u^{(1)}, v^{(1)}$, and η . Employing this data processing methodology for the three records would yield six expressions (18) for any pair of m and l . The first auto-spectrum equation $S_{\eta\eta}$ denotes the energy spectrum S_{ω} . It is employed in scaling all the other expressions. The equations are arranged in a linear matrix form to solve \hat{a}_n, \hat{b}_n coefficients per frequency,

$$\begin{bmatrix} a_{1\eta u} & b_{1\eta u} & a_{2\eta u} & b_{2\eta u} \\ a_{1\eta v} & b_{1\eta v} & a_{2\eta v} & b_{2\eta v} \\ a_{1uu} - a_{1vv} & b_{1uu} - b_{1vv} & a_{2uu} - a_{2vv} & b_{2uu} - b_{2vv} \\ a_{1uv} & b_{1uv} & a_{2uv} & b_{2uv} \end{bmatrix}_{\omega} \begin{bmatrix} \hat{a}_1 \\ \hat{b}_1 \\ \hat{a}_2 \\ \hat{b}_2 \end{bmatrix}_{\omega} = \begin{bmatrix} \frac{S_{\eta u}}{S_{\omega} \Delta\theta} - a_{0,\eta u} \\ \frac{S_{\eta v}}{S_{\omega} \Delta\theta} - a_{0,\eta v} \\ \frac{S_{uu} - S_{vv}}{S_{\omega} \Delta\theta} - (a_{0,uu} - a_{0,vv}) \\ \frac{S_{uv}}{S_{\omega} \Delta\theta} - a_{0,uv} \end{bmatrix}_{\omega}. \quad (20)$$

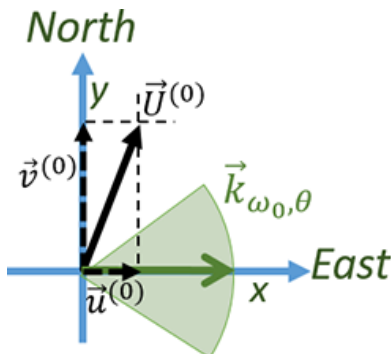


FIG. 2. Simulation setup. $k_{\omega_0, \theta}$ is the predetermined single-frequency wave spread according to Longuet-Higgins-Mitsuyasu where the mean direction is $\theta = 0^\circ$, and $\vec{U}^{(0)}$ is the ambient current direction projected on x and y in 1 : 3 ratio as $\vec{u}^{(0)}$, $\vec{v}^{(0)}$, respectively.

Here,

$$a_{0,ml} = \frac{1}{2\pi} \sum_{\theta} [H_m^s]_{\omega, \theta, z} [H_l^{s*}]_{\omega, \theta, z}, \quad (21)$$

$$a_{n,ml} = \frac{1}{\pi} \sum_{\theta} [H_m^s]_{\omega, \theta, z} [H_l^{s*}]_{\omega, \theta, z} \cos n\theta, \quad (22)$$

$$b_{n,ml} = \frac{1}{\pi} \sum_{\theta} [H_m^s]_{\omega, \theta, z} [H_l^{s*}]_{\omega, \theta, z} \sin n\theta. \quad (23)$$

There are five possible equations and only four unknowns ($n = 2$). The auto-spectra S_{uu} , S_{vv} can be combined into one equation $S_{uu} - S_{vv}$ as can be seen in the matrix third row (20). It is followed from the derivation of \hat{a}_2 in the potential approximation. Without a shearing current profile, the solution of the Fourier coefficients degenerates to the potential solution [7]. Thus, the total number of equations is four. The estimated mean wave direction $\hat{\theta}_m$ is obtained according to the first-harmonic Fourier coefficients,

$$\hat{\theta}_m = \arctan \left(\frac{\hat{b}_1}{\hat{a}_1} \right). \quad (24)$$

The method for deriving the wave directional spectrum was tested for the case of single frequency (monochromatic) waves propagating over a constant bottom depth of $h = 25$ m. Waves of $T_0 = 12.8$ s ($f_0 = 0.78$ Hz) were simulated in the presence of an exponential ambient current profile defined as $|U^{(0)}| = (u^{(0)^2} + v^{(0)^2})^{1/2} = \exp(0.25 \text{ m}^{-1}z)$. $U^{(0)}$ was inclined to the waves mean propagation direction in 72° corresponding to 1 : 3 ratio of its horizontal components $u^{(0)}(z)$, $v^{(0)}(z)$. Wave energy of $30 \text{ m}^2/\text{Hz}$ was distributed to predetermined directions according to a spread function $G(\theta) = G_0 \cos^{2s}(\frac{\theta - \theta_0}{2})$ [3,30]. The wave mean direction θ_0 was set to 0° corresponding to waves propagating from west to east (Fig. 2). The power was set to $s = 10$ that leads to a relatively narrow band corresponding to wind waves.

The simulation was carried out in two stages. The first stage provided three data sets (ηuv) as could have been recorded by an ADCP instrument accounting for the ambient current profile. The wave amplitudes $\eta_{\omega, \theta}^{(1)}$ were calculated according to their relation to the directional density spectrum via $\eta_{\omega, \theta} = (2S_{\omega, \theta}^2 \Delta\omega \Delta\theta)^{1/2}$. These wave amplitudes and the ambient current profile $u^{(0)}$, $v^{(0)}$ were provided as the input for the simulation with the directional angular step given as $\Delta\theta = 1^\circ$. The BVP was solved using the Maple mathematical software for each direction. The numerical solution

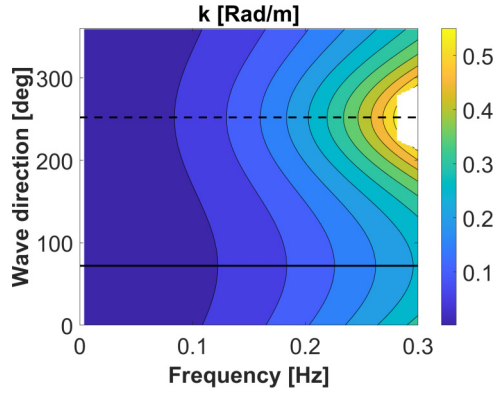


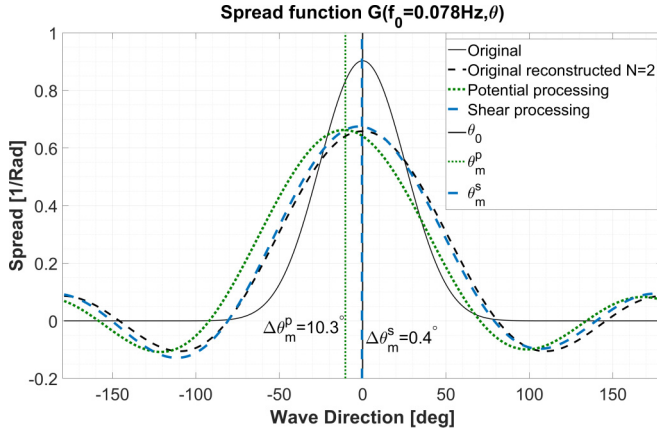
FIG. 3. Directional dispersion relation. The solid line indicates the current direction, while the dashed line is the opposite direction.

yielded the wave numbers $k_{\omega,\theta}$ and the vertical velocity profiles $w_{\omega,\theta}^{(1)}$. The vertical profiles were scaled according to their wave amplitudes. Then, the horizontal oscillatory velocities $u_{\omega,\theta}^{(1)}$, $v_{\omega,\theta}^{(1)}$ were calculated via (3).

The second stage included the data processing of the directional spectrum from the three data sets according to the derived methodology and the common potential methodology. Data sets of 2048 s requested to evaluate reliable spectra were sampled at a typical, for wind waves, sampling frequency of 2 Hz. The horizontal oscillatory velocities were computed at $z = z_0 = -2$ m ($\approx 0.1h$) as done in realistic ADCP measurement due to the inaccurate backscatter from the uppermost layer. The time series of the sea elevation $\eta(t)$, the east velocity $u(t)|_{z_0}$, and the north velocity $v(t)|_{z_0}$ were generated by employing an inverse fast Fourier transform (IFFT) with uniformly random phases $\phi_{\omega,\theta}$. The number of realizations was set to $N = 10\,000$ in order to eliminate, as much as possible, phase influence within the calculation time and computational limit and reduce the error of the wave spread function

$$\widehat{S}_{f,\theta} = \frac{1}{N} \sum_{i=1}^N (S_{f,\theta})_i. \quad (25)$$

The data processing for the generated data sets was carried out for all frequencies and all directions as in actual ADCP data processing. The estimation of the directional spread $\widehat{S}_{f,\theta}$ was carried out twice. The first estimation employed potential wave transfer functions, where the Fourier coefficients were calculated according to potential theory equations. The second estimation employed the new method while accounting for the ambient current velocity profile. The BVP was solved again, now for all wave frequencies and directions. This determined the complete dispersion relation cone and the rotational numerical transfer functions. The Fourier coefficients were solved according to the relations between the cross-spectra products (20)–(23). The dispersion relation cone for each frequency and direction is shown in Fig. 3. Figure 4 presents the spread functions for the case study. The black line indicates the original spread, and the dashed black line shows its reconstruction by accounting for Fourier coefficients of the input up to the second harmonics. This line provides the most accurate spread estimation which can be expected from analyzing triplet array of three independent records (η , u , v). The mean wave direction is determined by employing the first-harmonic coefficients (24), in accordance with its definition. The shape of the spread function may be improved when accounting for more harmonics (additional orders of Fourier coefficients), but it requires more sensors like in ADCP beam array data processing or clover leaf buoys along with an average current profile. However, the data processing with more sensors employed according to potential theory would yet suffer from the same biased mean wave direction. On the contrary,


 FIG. 4. Processed spread functions $G(f, \theta)$ of the single-frequency waves.

as explained in the paper, the mean direction is of utmost importance in many coastal problems, in particular in sediment transport. The dotted green line shows the spread obtained from the potential data processing, and the dashed blue line shows the spread obtained by the rotational data processing method accounting for the shearing current. The vertical lines indicate the corresponding mean direction. The difference between the original input mean direction to those obtained by the data processing are denoted as $\Delta\theta_m^p$ and $\Delta\theta_m^s$ for the potential and the shearing currents methods, respectively.

It can be clearly seen that the shearing current has an important role in acquiring a correct spread estimation. Ignoring its existence in potential data processing resulted in large errors with $\Delta\theta_m^p = 10.3^\circ$. This data processing methodology, which accounted for shearing current effects, provided a significantly more accurate spread estimation with a $\Delta\theta_m^s$ of only 0.4° together with an excellent and far superior agreement to the original reconstructed second-harmonic spread. The effect of the exponential current inclination compared with the mean wave direction on estimating the mean wave direction was tested for different inclinations in steps of 15° (Fig. 5). Note that the dispersion relation and the transfer functions are derived only according to the mean current profile (zero-order), and

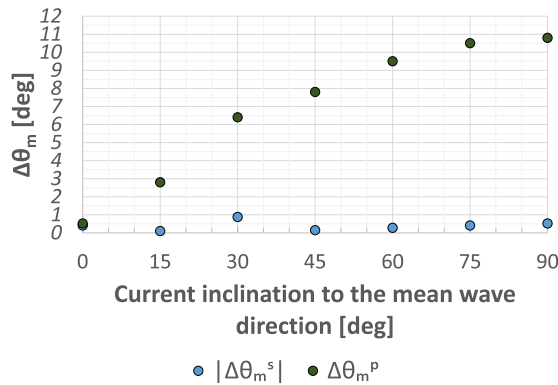


FIG. 5. Mean wave direction estimation error dependent on the exponential current inclination to the mean wave direction. As the perpendicular current component grows so is the error in the mean wave direction estimation. The small error variability with shear is due to the limited number of realizations and is less than $\Delta\theta$ for all inclinations, and is given in absolute value.

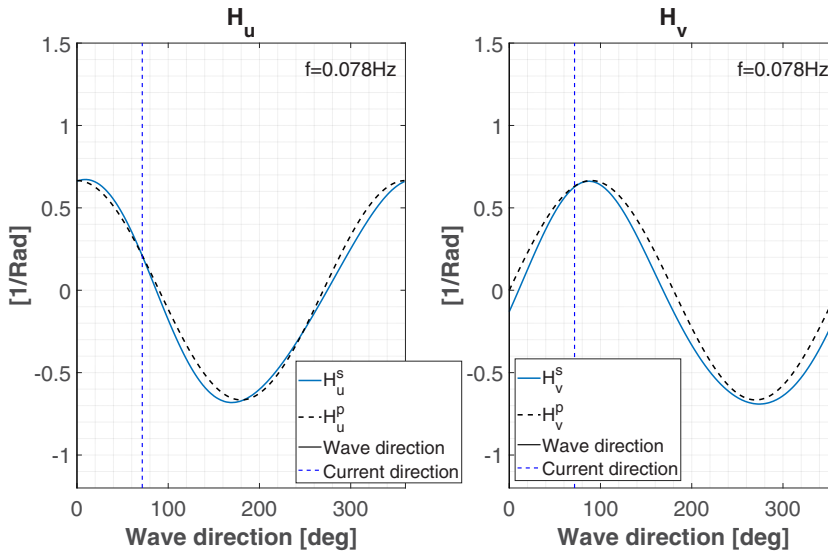


FIG. 6. Transfer functions H_u and H_v of the monochromatic wave.

that their solution is linear for any wave amplitude. The transfer functions for the monochromatic wave frequency are shown in Fig. 6. The significant differences between the rotational transfer functions H_u^s , H_v^s and their potential counterparts H_u^p , H_v^p both in shape and in magnitude explain the large differences between the obtained spreads.

The above findings reduce the confidence in validity of all wave data processing ever made for field measurements of pressure gauges, wave buoys, and ADCPs. The potential approximation is considered for many years as a reliable common practice in computing wave directional spectra estimations and is extensively used all over the world in field and laboratory measurements, and in calibration and validation of oceanic meteorological forecast models, and in coastal sediment transport models [31]. The ambient current data is commonly available in ADCP measurements. This allows us to reprocess their data with the derived method. When the ambient current conditions are not available, they can be evaluated from circulation models. Considering the inaccuracies of the commonly used potential methods, the reprocessing of years of historical data sets is apparently inevitable. This method has the potential to become a leading method for sensor data processing in maritime environment and in laboratories.

This research was supported by the Ministry of Innovation, Science and Technology, by the Israel Science Foundation [Grants No. 1940/14 and No. 1601/20], and the German-Israeli cooperation in Marine Science (BMBF-MOST) [Grant No. 3-15249]. Special thanks and our gratitude is expressed to MEng Valerie McKay-Crites, the Customer Success Engineer at Maplesoft, for her dedicated support in utilizing the boundary-value problem solver.

-
- [1] N. N. Panicker and L. E. Borgman, Directional spectra from wave-gage arrays, *Coast. Eng.* 117 (1970).
 - [2] N. N. Panicker, A. M. and L. E. Borgman, Enhancement of directional wave spectrum estimates, *Coast. Eng.* 258 (1974).
 - [3] M. S. Longuet-Higgins, D. E. Cartwright, and N. D. Smith, Observation of the directional spectrum of sea waves using the motion of a floating buoy, *Ocean wave spectra* (1963).

- [4] A. J. Kuik, G. Ph. Van Vledder, and L. H. Holthuijsen, A method for the routine analysis of pitch-and-roll buoy wave data, *J. phys. Ocean.* **18**, 1020 (1988).
- [5] E. J. Gumbel, J. A. Greenwood, and D. Durand, The circular normal distribution: Theory and tables, *J. Am. Stat. Assoc.* **48**, 131 (1953).
- [6] L. E. Borgman, Directional spectra models for design use, *Offshore Technology Conference* (OnePetro, 1969).
- [7] M. K. Ochi, *Ocean Waves: The Stochastic Approach* (Cambridge University Press, London, 1998), p. 332.
- [8] Y. Goda, *Random Seas and Design of Maritime Structures* (World Scientific Publishing Co. Pte. Ltd, Singapore, 2010), Vol. 15, pp. 1–462.
- [9] Datawell, Wave rider reference manual, dwr-mkiii. (Datawell BV Oceanographic Instruments, The Netherlands, 2009).
- [10] M. Donelan, A. Babanin, E. Sanina, and D. Chalikov, A comparison of methods for estimating directional spectra of surface waves, *J. Geophys. Res. C: Oceans* **120**, 5040 (2015).
- [11] J. Capon, R. J. Greenfield, and R. J. Kolker, Multidimensional maximum-likelihood processing of a large aperture seismic array, *Proc. IEEE* **55**, 192 (1967).
- [12] R. E. Davis and L. A. Regier, Methods for estimating directional wave spectra from multi-element arrays, *J. Mar. Res.* **35**, 453 (1977).
- [13] L. E. Borgman, Maximum-entropy and data-adaptive procedures in the investigation of ocean waves, in *Maximum-Entropy and Bayesian Methods in Inverse Problems*, Fundamental Theories of Physics, Vol. 14 (Springer, Dordrecht, 1985), pp. 429–442.
- [14] M. Isobe, K. Kondo, and K. Horikawa, Extension of MLM for estimating directional wave spectrum, in *Proc. Symp. on Description and Modeling of Directional Seas* (1984), pp. A-6-1–A-6-15.
- [15] H. E. Krogstad, Maximum likelihood estimation of ocean wave spectra from general arrays of wave gauges, *Model. Identific. Control* **9**, 81 (1988).
- [16] L. Aouf, J.-M. Lefèvre, and D. Hauser, Assimilation of directional wave spectra in the wave model WAM: An impact study from synthetic observations in preparation for the swimsat satellite mission, *J. Atmos. Ocean. Technol.* **23**, 448 (2006).
- [17] I. Houghton, P. Smit, D. Clark, C. Dunning, A. Fisher, N. Nidzicko, P. Chamberlain, and T. Janssen, Performance statistics of a real-time pacific ocean weather sensor network, *J. Atmos. Ocean. Technol.* **38**, 1047 (2021).
- [18] K. Raghukumar, G. Chang, F. Spada, C. Jones, T. Janssen, and A. Gans, Performance characteristics of "spotter," a newly developed real-time wave measurement buoy, *J. Atmos. Ocean. Technol.* **36**, 1127 (2019).
- [19] P. Smit, I. Houghton, K. Jordanova, T. Portwood, E. Shapiro, D. Clark, M. Sosa, and T. Janssen, Assimilation of significant wave height from distributed ocean wave sensors, *Ocean Model.* **159**, 101738 (2021).
- [20] I. A. Houghton, C. Hegermiller, C. Teicheira, and P. B. Smit, Operational assimilation of spectral wave data from the sofar spotter network, *Geophys. Res. Lett.* **49**, e2022GL098973 (2022).
- [21] R. H. Stewart and J. W. Joy, HF radio measurements of surface currents, *Deep Sea Research and Oceanographic Abstracts* (Elsevier, 1974), Vol. 21, pp. 1039–1049.
- [22] O. Klein, E. Heifetz, and Y. Toledo, Surface gravity waves in the presence of vertically shearing current and eddy viscosity, *Phys. Fluids* (2022).
- [23] Z. Zheng, Y. Li, and S. Å. Ellingsen, Statistics of weakly nonlinear waves on currents with strong vertical shear, *Phys. Rev. Fluids* **8**, 014801 (2023).
- [24] Z. Zheng, Y. Li, and S. Ellingsen, Extreme waves on vertically sheared flows: Statistical analysis of weakly nonlinear waves, in *EGU General Assembly Conference Abstracts, Vienna, Austria* (2022), pp. EGU22-8285.
- [25] S. Å. Ellingsen and Y. Li, Approximate dispersion relations for waves on arbitrary shear flows, *J. Geophys. Res. Oceans* **122**, 9889 (2017).
- [26] See Supplemental Material at <http://link.aps.org/supplemental/10.1103/PhysRevFluids.8.L062801> for general description of wave data processing and on the Rayleigh boundary-value problem based on the the wave rotational theory.

- [27] A. G. Voronovich, Propagation of internal and surface waves in geometrical optics approximation, *Izv. Atmos. Ocean. Phys.* **12**, 850 (1976).
- [28] L. Vitkin, D. Liberzon, B. Grits, and E. Kit, Study of in situ calibration performance of co-located multi-sensor hot-film and sonic anemometers using a ‘virtual probe’ algorithm, *Meas. Sci. Technol.* **25**, 075801 (2014).
- [29] E. Kit and D. Liberzon, 3D-calibration of three-and four-sensor hot-film probes based on collocated sonic using neural networks, *Meas. Sci. Technol.* **27**, 095901 (2016).
- [30] H. Mitsuyasu, F. Tasai, T. Suhara, S. Mizuno, M. Ohkusu, T. Honda, and K. Rikiishi, Observations of the directional spectrum of ocean waves using a cloverleaf buoy, *J. Phys. Oceanogr.* **5**, 750 (1975).
- [31] A. Perlin and E. Kit, Longshore sediment transport on mediterranean coast of Israel, *J. Waterway, Port, Coastal, Ocean Eng.* **125**, 80 (1999).